

# Reactive Power Control for Single-phase Grid-tie Inverters using Quasi Sinusoidal Waveform

Dong Li, *Student Member, IEEE*, Carl Ngai Man Ho, *Senior Member, IEEE*, Luo Liu, Gerardo Escobar, *Senior Member, IEEE*

**Abstract**— The paper presents a reactive power control technique for single-phase Photovoltaic (PV) inverters, especially unfolding inverters. The proposed system retains the benefit of the unfolding inverters having low material cost and semiconductor losses, and tackles the drawback of the standard unfolding inverter not having capability of reactive power injection. It is important to note that reactive power delivery is mandatory for PV inverters according to the recent announced regulations. The concept is based on changing the shape of the grid current waveform but keeping the same zero crossing points as in the unity power factor condition. The current waveform is governed by real power and reactive power, at the price of an acceptable deformation. The operating principles of the proposed technique and mathematical derivations of the grid current function are provided in the paper. Experimental results in a grid-tie inverter prototype have shown a good agreement with the derived theory, and they confirm the feasibility of using the proposed technique in grid-tie inverters.

**Keywords**— Photovoltaic, Inverter, Reactive Power, Power Factor

## I. INTRODUCTION

Unfolding grid-tie inverters are generally used in Photovoltaic (PV) and Fuel Cell (FC) applications [2]-[9]. This is because a simple controller can be applied and it can minimize the number of high frequency switching semiconductors, e.g. MOSFETs. This leads to low component cost and high efficiency. Fig. 1 shows a typical system block diagram of an unfolding grid-tie inverter [4]. The front stage is a dc-dc converter, which converts a dc current from a voltage source, such as PV Cells, to a rectified sinusoidal inductor current. The second stage is a line frequency inverter to unfold the inductor current into a bipolar sinewave current, which is synchronized with the grid voltage [10]-[12]. Typically, semiconductor switches in the line frequency inverter are SCR thyristors [10]. It is well-known that SCR are turned off at zero current with relatively long commutation time which makes difficult for the injection of reactive power. Thus, the impossibility of injecting

D. Li, C.N.M. Ho (Corresponding author) and L. Luo are with the RIGA Lab, the Department of Electrical & Computer Engineering, University of Manitoba, R3T5V6, Winnipeg, MB, Canada (E-mail: carl.ho@umanitoba.ca).

G. Escobar is with the Engineering School, Universidad Autonoma del Carmen, 24180 Cd. del Carmen, Campeche, Mexico (e-mail: gescobar@ieee.org).

This is an updated version of conference paper [1]. This new version includes benchmarking of different waveforms, updated experimental results. Text and equations have been thoroughly revised as well.

The work described in this paper was fully supported by a grant from the Canada Research Chairs, Canada (Sponsor ID: 950-230361).

reactive power is the main drawback of unfolding inverters. However, a new regulation has been recently published to require that PV inverter products must have the capability to adjust Power Factor (PF) up to 0.95 in either inductive or capacitive modes [13], [14]. In consequence, a lot of already designed commercial products are facing the problem of not passing such a regulation. Some advanced modulation methods have been proposed recently to satisfy the PF regulation [15], [16], but they cannot be applied to unfolding inverters since the zero crossing points of grid voltage and current are not the same. Thus, manufacturers have to redesign PV inverter system completely using different semiconductors or changing topology to be more complicated and expensive such as Neutral Point Clamped (NPC) inverters to satisfy the regulation in their future products.

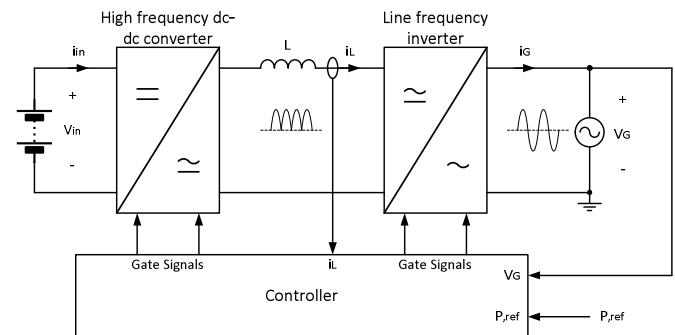


Fig. 1 A typical single-phase grid-tie unfolding inverter system.

Beside the regulation, unfolding inverters give a high efficiency when using MOSFETs in the line frequency inverter stage instead of SCRs. A commercial single phase PV inverter system can achieve 97.8% European efficiency with using Silicon MOSFETs only in the inverter stage [17]. The MOSFETs effectively reduce the conduction loss comparing to SCRs. However, the zero crossing points of grid current and grid voltage have to be synchronized, otherwise it will produce a short circuit path by the body diodes, otherwise, a cascaded blocking diode is required for each MOSFET. The high efficiency advantage does not exist anymore due to a high conduction loss at the diodes [18]. Nevertheless, reactive power cannot be delivered to the grid. A manufacturer has provided a solution which changes the shape of the grid current waveform to give a capability of generating 0.95 power factor [19]. However, there are no further literatures to provide the operating principles and the performance evaluations by using the method.

This paper follows up the idea in the literature [19] to propose a control technique for grid-tie inverters, especially unfolding inverters. The delivered grid current is modified to the proposed Quasi Sinusoidal Waveform (QSW) to carry reactive power, and thus satisfying the PF regulations. The modified current keeps the same zero crossing points as the grid voltage. The injection of reactive power is thus possible at the expenses of an acceptable current shape deformation. Although it contains harmonics during reactive power delivering and it is the drawback of the proposed waveform, the total harmonic distortion (THD) is relatively low. Recall that, during unity power factor, the current satisfies the THD regulation such as IEC61000-3-2 [20]. This paper provides the mathematical derivation of the proposed grid current reference function. Numerical and experimental results of the proposed technique applied to an grid-tie inverter are presented to verify the theoretical findings.

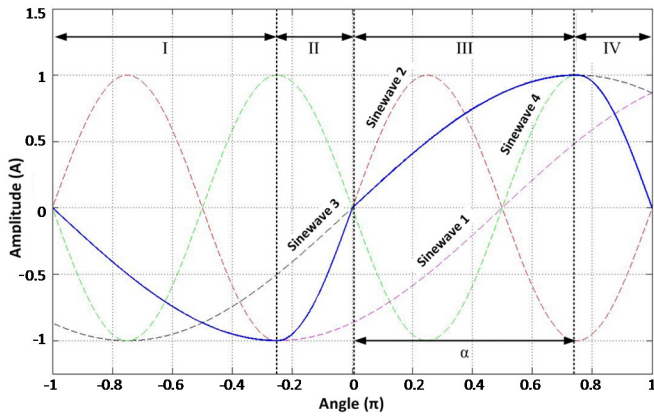


Fig. 2 Proposed Quasi Sinusoidal Waveform.

## II. STEADY STATE CHARACTERISTICS

### A. Ideal Quasi Sinusoidal Waveform

In this paper, Quasi Sinusoidal Waveform (QSW) is defined as a waveform which is formed by sinusoidal waveforms with different frequencies. The resultant waveform is close to a sine wave but it includes harmonics in the signal. Fig. 2 shows the proposed QSW signal indicated by a solid blue line, which is proposed as the reference for the delivered grid current. This waveform is divided into 4 time intervals, where the boundaries are fixed at peaks and zero crossings of this waveform. Notice that each interval consists of a fraction of a sine function that frequency alternates between two different values. The mathematical expression of such a composed function is given by,

$$f(t) = \begin{cases} -A \sin \frac{\omega t + \pi}{2\alpha}, & -\pi \leq \omega t < -(1-\alpha)\pi \\ A \sin \frac{\omega t}{2(1-\alpha)}, & -(1-\alpha)\pi \leq \omega t < 0 \\ A \sin \frac{\omega t}{2\alpha}, & 0 \leq \omega t < \alpha\pi \\ -A \sin \frac{\omega t - \pi}{2(1-\alpha)}, & \alpha\pi \leq \omega t < \pi \end{cases} \quad (1)$$

where  $\alpha$  adjusts the shape of the curve and is referred as adjusting ratio. For instance, in Fig. 2,  $\alpha$  is set to 0.75.  $A$  is peak

value and  $T$  is period. Fig. 3 shows QSW signals with different  $\alpha$ . Notice that, for  $\alpha = 0.5$ , a regular sinusoidal waveform is generated, otherwise the peaks of the waveform are shifted.

The frequency of sinusoidal waves that constitute QSW in each interval can be determined by resultant QSW signal frequency  $f_Q$  and  $\alpha$  as,

$$f_I = f_{III} = \frac{f_Q}{2\alpha} \quad (2)$$

and

$$f_{II} = f_{IV} = \frac{f_Q}{2(1-\alpha)} \quad (3)$$

These two variables,  $\alpha$  and  $A$ , in (1) are used to adjust power factor and current amplitude of a current injecting into a grid. Fig. 3 shows a QSW with different  $\alpha$ . When  $\alpha$  is 0.5, it is a pure sinusoidal waveform, otherwise the peaks of the waveform are shifted. In the graph can be seen that the resultant frequency, and zero crossing points of waveforms are the same.

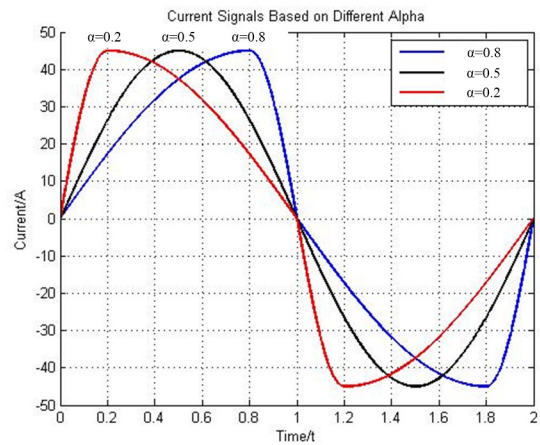


Fig. 3 Quasi Sinusoidal Waveform with different  $\alpha$ .

### B. Fourier Series of Quasi Sinusoidal Waveform

In order to determine the periodic signal function of the QSW, the method of Fourier series is used [21]. The current reference,  $i(t)$ , with QSW can be represented by the following equation,

$$i(t) = \sum_{n=1}^{\infty} (a_n \cos n\omega t + b_n \sin n\omega t) \quad (4)$$

where  $n$  is the number of harmonic of the current,  $\omega$  is the angular frequency, and

$$a_n = \frac{2A}{\pi} \cdot K_n \cdot [1 - 4n^2\alpha(\alpha - 1) - 2n \sin(\alpha n\pi)] \quad (5)$$

$$b_n = \frac{2A}{\pi} \cdot K_n \cdot 2n \cos(\alpha n\pi) \quad (6)$$

and  $K_n$  is,

$$K_n = \frac{[1 - (-1)^n] \cdot (2\alpha - 1)}{\{[2n(\alpha - 1)]^2 - 1\} \cdot [(2n\alpha)^2 - 1]} \quad (7)$$

A detailed derivation of (4) – (7) is given in the Appendix.

According to the questions,  $a_n$  and  $b_n$  are function of amplitude of QSW waveform,  $A$ , and the control coefficient,  $\alpha$ . Thus, the waveform can be adjusted by those two parameters.

A periodic signal can be expanded to a fundamental frequency and harmonics. The general form is represented by,

$$i(t) = \sum_{n=1}^{\infty} I_n \sin(n\omega t + \theta_n) \quad (8)$$

where  $I_n$  is magnitude and  $\theta_n$  is phase angle. The parameters can be determined by,

$$I_n = \sqrt{a_n^2 + b_n^2} \quad (9)$$

$$\theta_n = \tan^{-1} \left( \frac{a_n}{b_n} \right) \quad (10)$$

A detailed derivation of (9) – (10) is given in the Appendix.

By putting (5), (6) into (9) and (10),  $I_n$  and  $\theta_n$  can be expressed by  $A$  and  $\alpha$  as,

$$I_n = \frac{2A}{\pi} \cdot K_n \cdot \sqrt{[1 - 4n^2\alpha(\alpha-1) - 2n \sin(\alpha n\pi)]^2 + [2n \cos(\alpha n\pi)]^2} \quad (11)$$

$$\theta_n = \tan^{-1} \left( \frac{1 - 4n^2\alpha(\alpha-1) - 2n \sin(\alpha n\pi)}{2n \cos(\alpha n\pi)} \right) \quad (12)$$

All harmonic components can be determined based on (7), (11) and (12) by simply assigning values of  $n$ ,  $A$  and  $\alpha$ .

### C. Electrical Performance Characteristics

Furthermore, Total Harmonic Distortion (THD), Power Factor (PF), Real Power (P) and Reactive Power (Q) can be determined based on the parameters of the fundamental component and harmonic components of the current reference.

#### 1) Total Harmonic Distortion (THD) and Power Factor (PF)

The general equations for total harmonic distortion (THD) [22] and power factor (PF) [23] are,

$$THD = \frac{\sqrt{\sum_{n=3}^{\infty} I_n^2}}{I_1} \quad (13)$$

$$PF = \frac{1}{\sqrt{1+THD^2}} \cos \theta_1 \quad (14)$$

By putting (11) into (13), the THD equation can be rewritten as,

$$THD = \frac{\sqrt{\sum_{n=3}^{\infty} K_n^2 \{ [1 - 4n^2\alpha(\alpha-1) - 2n \sin(\alpha n\pi)]^2 + [2n \cos(\alpha n\pi)]^2 \}}}{K_1 \cdot \sqrt{[1 - 4\alpha(\alpha-1) - 2 \sin(\alpha\pi)]^2 + [2 \cos(\alpha\pi)]^2}} \quad (15)$$

where  $K_1$  is a term by assigning  $n = 1$  in (7).

According to (15), THD is independent of amplitude  $A$ . The THD variation with changing  $\alpha$  can be obtained and illustrated in Fig. 4. It can be seen in Fig. 4 that QSW gives the lowest THD (pure sine wave) when  $\alpha = 0.5$ . It increases propositionally when  $\alpha$  moves to left or right.

By putting equations (12) and (15) into (14), the PF equation can be rewritten as,

$$PF = \frac{4 \cos(\alpha\pi) \cdot \sqrt{\sum_{n=1}^{\infty} K_n^2 \{ [1 - 4n^2\alpha(\alpha-1) - 2n \sin(\alpha n\pi)]^2 + [2n \cos(\alpha n\pi)]^2 \}}}{[4(\alpha-1)^2 - 1] \cdot (2\alpha+1)} \quad (16)$$

Fig. 5 illustrates the PF variation with changing  $\alpha$ . It can be seen that QSW gives  $PF = 1$  when  $\alpha = 0.5$ . It decreases when  $\alpha$  moves to left or right. And it can reach  $PF = 0.95$  when  $\alpha = 0.22$  or  $0.78$ .

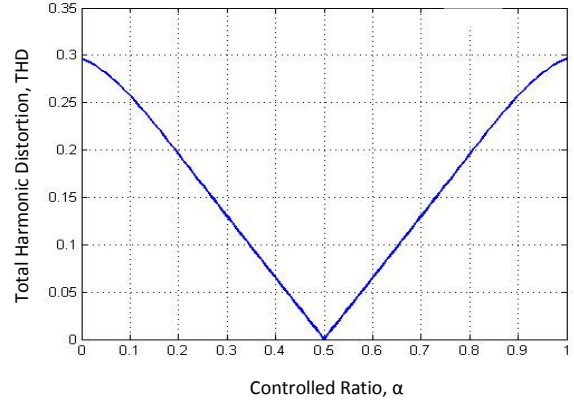


Fig. 4 THD changes based on different  $\alpha$ .

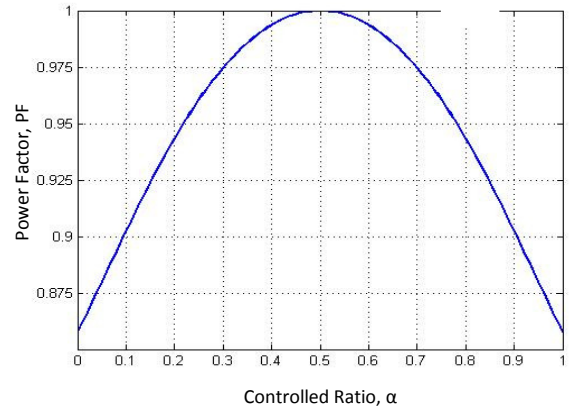


Fig. 5 Power factor changes based on different  $\alpha$ .

#### 2) Real Power (P) and Reactive Power (Q)

Based on the power transfer theory, the real power is defined as,

$$P = \frac{V_s I_1}{2} \cos \theta_1 \quad (17)$$

By putting  $b_n$  in (6) with  $n = 1$  into (17), the relationship of  $b_n$  and the fundamental component is shown in (A8), the real power equation can be rewritten as,

$$P = \frac{2A}{\pi} \cdot \frac{2V_s \cos(\alpha\pi)}{[4(\alpha-1)^2 - 1] \cdot (2\alpha+1)} \quad (18)$$

Based on the power transfer theory, the reactive power is defined as,

$$Q = \frac{V_s I_1}{2} \sin \theta_1 \quad (19)$$

By putting  $a_n$  in (5) with  $n = 1$  into (19), the relationship of  $b_n$  and the fundamental component is shown in (A7), the reactive power equation can be rewritten as,

$$Q = \frac{2A}{\pi} \cdot \frac{V_s \cdot [1 - 4\alpha(\alpha - 1) - 2\sin(\alpha\pi)]}{[4(\alpha - 1)^2 - 1](2\alpha + 1)} \quad (20)$$

Based on (18) and (20), the steady-state characteristics of the real and the reactive powers can be obtained by putting the variables  $A$  and  $\alpha$ .

### III. BENCHMARKING SIMILAR WAVEFORMS

In order to reduce THD while generating reactive power, three different types of waveform were analyzed and compared as shown in Fig. 6. For Quasi Sinusoidal Waveform (QSW), we have discussed in detail before. The method for controlling reactive power is to insert a control factor  $\alpha$  that can shift the first order harmonic of the current signal by adjusting the shape slant. By using the same control technique, it might be also possible to use four parts of line segment or four parts of parabola to achieve that. (21) and (22) are equations for Parabola Combined Waveform and Line Segments Combined Waveform, respectively. Corresponding waveforms are shown in Fig. 6.

Equations of Parabola Combined Waveform:

$$f(t) = \begin{cases} A \cdot \left\{ \frac{[t + (1-\alpha)\frac{T}{2}]^2}{(-\alpha\frac{T}{2})^2} - 1 \right\}, & -\frac{T}{2} \leq t < -(1-\alpha)\frac{T}{2} \\ A \cdot \left\{ \frac{[t + (1-\alpha)\frac{T}{2}]^2}{[(1-\alpha)\frac{T}{2}]^2} - 1 \right\}, & -(1-\alpha)\frac{T}{2} \leq t < 0 \\ A \cdot \left\{ 1 - \frac{[t - \alpha\frac{T}{2}]^2}{(-\alpha\frac{T}{2})^2} \right\}, & 0 \leq t < \alpha\frac{T}{2} \\ A \cdot \left\{ 1 - \frac{[t - \alpha\frac{T}{2}]^2}{[(1-\alpha)\frac{T}{2}]^2} \right\}, & \alpha\frac{T}{2} \leq t < \frac{T}{2} \end{cases} \quad (21)$$

Equations of Line Segments Combined Waveform:

$$f(t) = \begin{cases} -\frac{2A}{\alpha T}t - \frac{A}{\alpha}, & -\frac{T}{2} \leq t < -(1-\alpha)\frac{T}{2} \\ \frac{2A}{(1-\alpha)T}t, & -(1-\alpha)\frac{T}{2} \leq t < 0 \\ \frac{2A}{\alpha T}t, & 0 \leq t < \alpha\frac{T}{2} \\ -\frac{2A}{(1-\alpha)T}t + \frac{A}{1-\alpha}, & \alpha\frac{T}{2} \leq t < \frac{T}{2} \end{cases} \quad (22)$$

By using the same approach in Section II with the equations (4) - (20), the Steady-state characteristics of THD and PF can be determined for those two waveforms, Parabola Combined Waveform and Line Segments Combined Waveform, with different  $\alpha$ . Fig. 6 shows the shape of those three benchmarked waveforms when all three waveforms have the same peak value,  $A$ , and control factor,  $\alpha$ . And it can be observed that the current value of QSW waveform is always in between another two waveforms beside the zero-crossing and the peak points. Fig. 7 shows the  $\alpha$ -THD relationship of those three waveforms. It can be seen that, in the region near  $\alpha=0.5$ , QSW has a significant lower THD. It means that only QSW can generate pure sinusoidal waveform. Fig. 8 shows the  $\alpha$ -PF relationship of the benchmarked waveforms. Though Line Segments Combined Waveform has a larger controllable PF range, it cannot reach PF=1. It means it cannot generate unity power factor since THD of Line Segment Combined Waveform is

relatively high and PF is function of THD according to (14). But Parabola Waveform and QSW do have that problem since lower THD when  $\alpha=0.5$ .

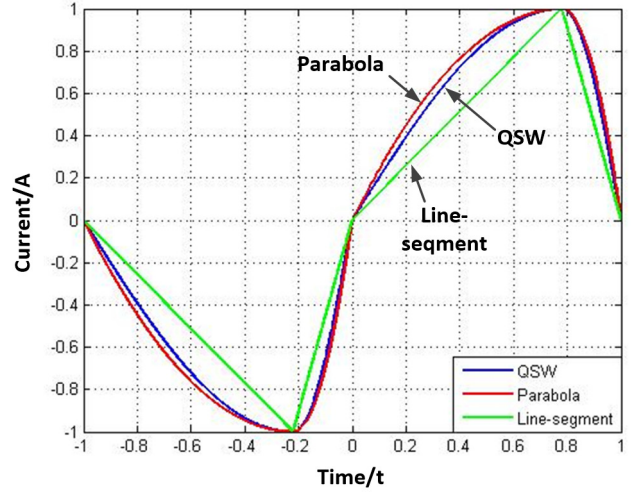


Fig. 6 Comparison of three types of waveform

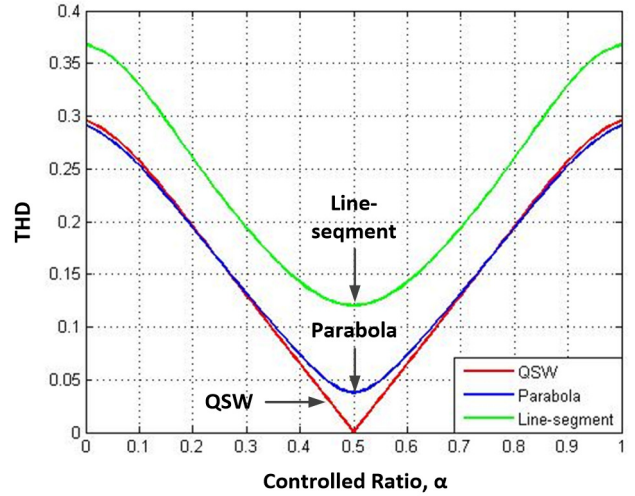


Fig. 7 Comparison of THD relationships

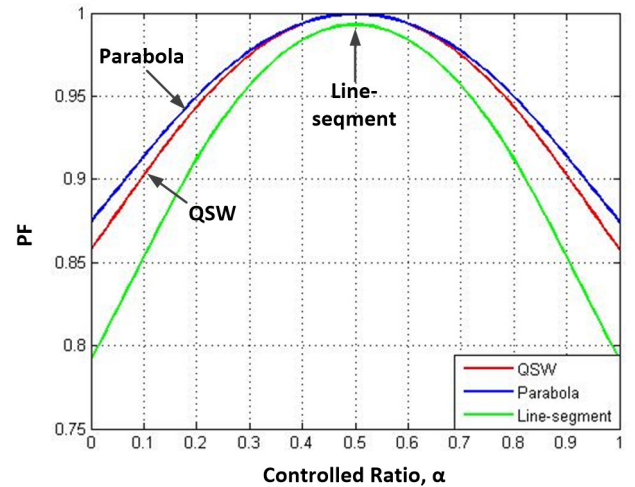


Fig. 8 Comparison of power factor relationships

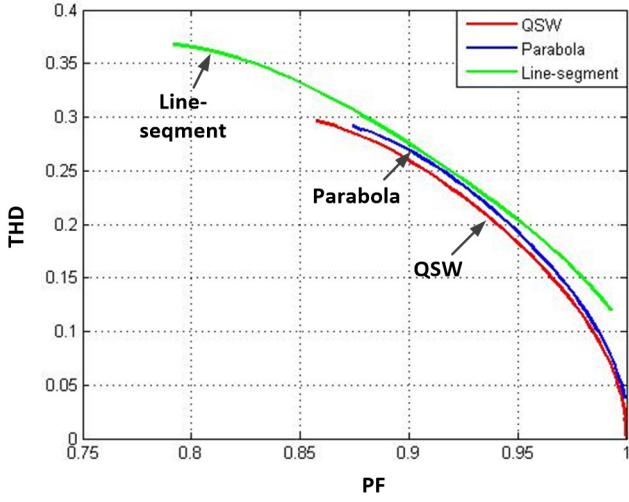


Fig. 9 Comparison of THD&PF relationships

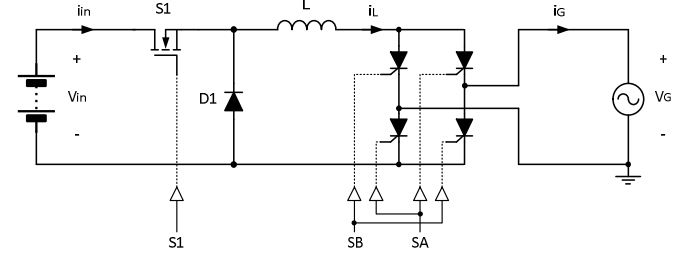
The goal for this control technique is to achieve reactive power injection with relatively low THD. As shown in Fig. 9, with same power factor, QSW signal always has the lowest THD among those three waveforms. QSW also has advantage that the property of sinusoids is widely used in many phase control cases. QSW can achieve a THD of 0 and the PF can be controlled in a relatively big range from 0.86~1. Above all, the proposed waveform, Quasi Sinusoidal Waveform, has ability to shift phase of its first order harmonic with relatively low THD.

#### IV. CONTROLLER DESIGN AND IMPLEMENTATION

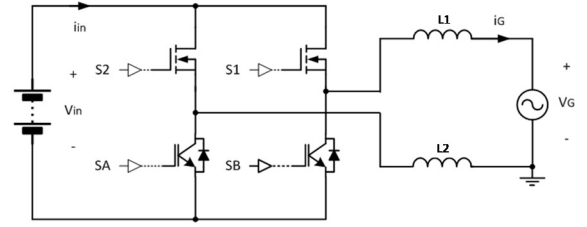
The concept of proposed control is to keep the zero crossing points of grid current and voltage to be the same, but shift the first order component of grid current to carry reactive power. The ideal grid current waveform was shown in Fig. 2. Since the zero crossing points are the same as those of grid voltage, this same reference can be applied to various types of inverter to inject reactive power into the grid. Fig. 10 (a) and (b) show two typical grid-tie inverters, an unfolding inverter and a unipolar switching full-bridge inverter [24], respectively. The typical gate signals of two converters are identical, SA and SB switch with the line frequency, e.g. 60 Hz, and S1 and S2 switch at a high frequency, e.g. 20 kHz, to shape the inductor current. It is well known that these inverters cannot deliver reactive power or generate considerably large switching losses under standard controllers. By using the proposed technique, these topologies do not require to change any hardware components. In fact, it is only required to add a current reference generator in the control loop to produce the QSW current reference.

Fig. 11 (a) is a typical control diagram for inverters in Fig. 10 with no reactive power control [25]. The current reference is given by a sinusoidal waveform which is generated by a Phase-Locked-Loop (PLL) with a synchronization of grid voltage, and sometimes the current reference is from sensed grid voltage directly. Fig. 11 (b) shows the proposed controller block diagram, where QSW current reference generator has been introduced. The dash-line blocks illustrate the modifications of the original control loop. Firstly, a QSW reference generator replaces the simple sinusoidal wave generator. There are two parts in the generator, a sinusoidal wave generator and a

controller to transform sinusoidal wave into the QSW. The sinusoidal wave generator gives a sinusoidal wave which is synchronized with the grid voltage through a PLL. Therefore, based on this synchronized signal, doing some transformation to generate QSW current reference can promise the output QSW current well synchronized with the grid voltage. Secondly, as shown in blue block, for the feed-forward control, original grid voltage should also be processed to QSW shape.

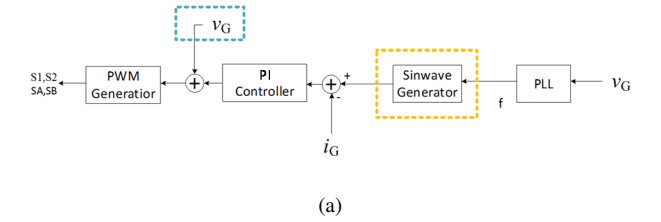


(a)

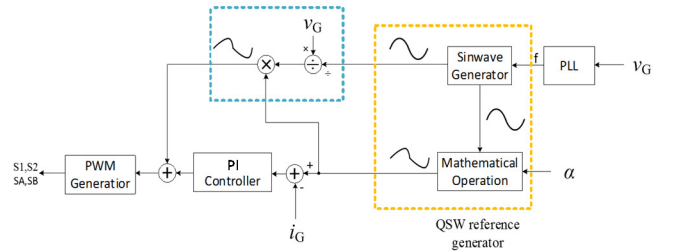


(b)

Fig. 10 Typical grid-tie inverter topologies: (a) unfolding inverter, and (b) unipolar switching full-bridge inverter.



(a)



(b)

Fig. 11 Control block diagrams: (a) A typical inverter controller, and (b) controller implementation to guarantee a QSW grid current.

The transformation from a pure sinusoidal wave to QSW only is a simple process. Firstly, based on the value and the slope of a sinusoidal wave, the phase information,  $\omega t$ , can be obtained by using inverse trigonometric computation. Then, the QSW reference value can be calculated using equation (1) with  $\omega t$ .

Trigonometric and inverse trigonometric computation can be performed accurately and quickly by any DSP or micro-controller in real time.

The proposed control technique modified the current reference waveforms, which means it does not change anything in small signal analysis. Hence the design of PI controller in Fig. 11 (b) can be kept as same as the original controller in Fig. 11 (a).

TABLE I. SPECIFICATION

Parameter	Value	Parameter	Value
$V_G$	120V	$V_{DC}$	380V
$P_O$	800W	$f_{sw}$	20kHz
$L_1, L_2$	2.0mH		

### V. EXPERIMENTAL VERIFICATIONS

The performance of the proposed controller has been experimentally demonstrated in a prototype of a full-bridge inverter. For the inverter system, a 800W/120V inverter was built, which is a full-bridge inverter with unipolar SPWM, controlled by a TI F28377s DSP. The inverter has the same topology as shown in Fig. 10 (b). Table I shows the specification of this inverter. In the testbed, DC source voltage is set to be 380V as input voltage of the inverter, AC voltage source which represents grid to be 120V and the peak value of QSW current reference is set to be 9A. Fig. 12 shows the connection diagram of experimental test setup and Fig. 13 shows the actual testbed. Fig. 14 shows the waveforms of grid current when  $\alpha$  is set at 0.22, 0.5 and 0.78.

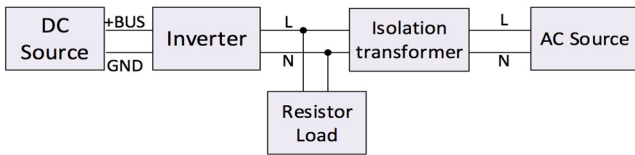


Fig. 12 Experimental test connection diagram.

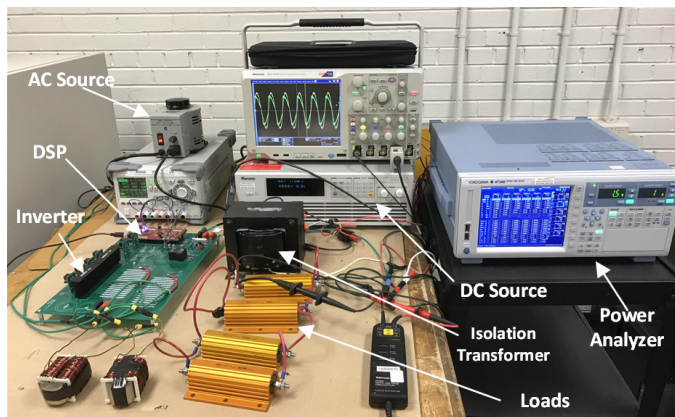
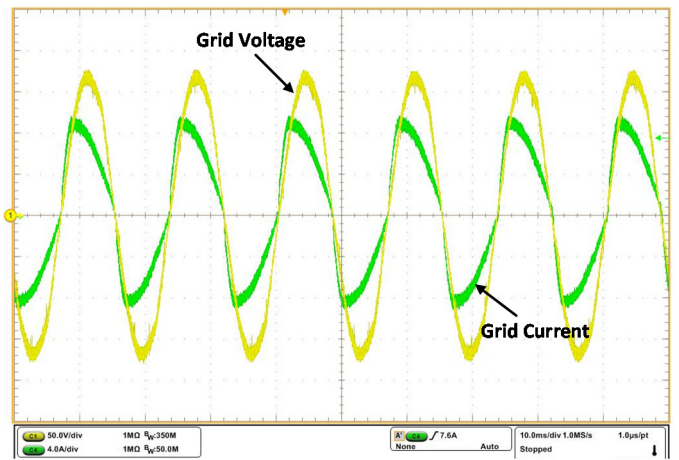
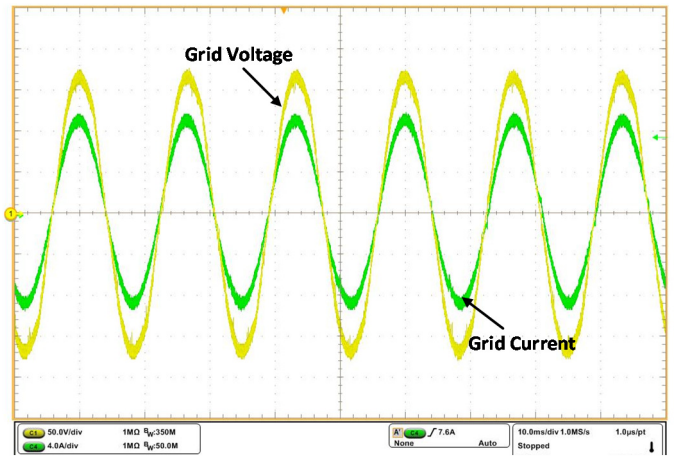


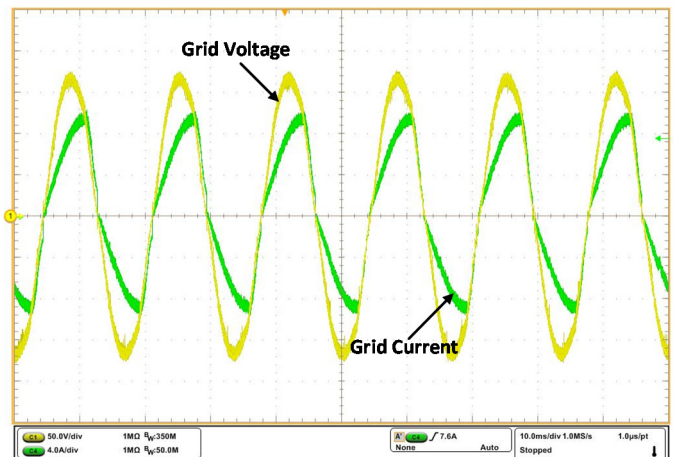
Fig. 13 Experimental test setup.



(a)



(b)



(c)

Fig. 14 Steady state responses of delivered grid current and grid voltage for different values of  $\alpha$ : (a)  $\alpha = 0.22$ , (b)  $\alpha = 0.5$ , and (c)  $\alpha = 0.78$ .

According to (16) and Fig. 5, when  $\alpha$  is set to 0.22, 0.5 and 0.78, theoretically the power factor should be 0.95, 1.0 and 0.95, respectively. Table II shows the power parameters of corresponding waveforms in Fig. 14 measured by a power analyzer. It shows that the measured power factors are very close to the theoretical results. This means that it is possible to generate reactive power using QSW current, and control the

power factor by selecting deferent  $\alpha$  value. Besides the waveforms show that the proposed control method has the ability to produce an expected QSW current which is well synchronized to grid voltage, and the zero-crossing points of grid voltage and QSW current are accurately locked. This fact promises that the proposed technology can be applied on unfold inverters as shown in Fig. 10.

TABLE II. EXPERIMENTAL RESULTS

$\alpha$	Apparent Power $S$	Active Power $P$	Power Factor $\lambda$
0.22	756.4VA	718.3W	0.9492
0.50	757.1VA	755.2W	0.9982
0.78	767.2VA	732.0W	0.9534

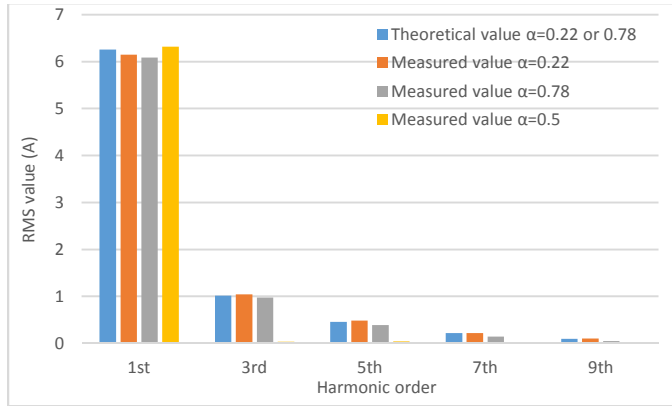


Fig. 15 Harmonic analysis of test QSW current.

TABLE III. COMPARISON OF HARMONIC MAGNITUDES

	1st	3rd	5th	7th	9th
Theoretical value (A) $\alpha = 0.22$ or $0.78$	6.260	1.015	0.459	0.221	0.095
Measured value (A) $\alpha = 0.22$	6.150	1.041	0.486	0.217	0.102
Measured value (A) $\alpha = 0.78$	6.309	0.976	0.391	0.141	0.051

Fig. 15 shows the measured harmonic values compared with theoretical values. It can be seen that, when set  $\alpha = 0.5$ , the fundamental current is dominating in the frequency spectrum, it means it is very close to a pure sinusoidal wave. In contrast, when  $\alpha = 0.78$  or  $0.22$ , it contains extra 3<sup>rd</sup>, 5<sup>th</sup>, 7<sup>th</sup> and 9<sup>th</sup> harmonics. Table III shows the comparison of measured harmonic RMS values and theoretical harmonic RMS values. According to the IEC61000-3-2 standard, all harmonic current amplitudes are with the limits. Furthermore, the comparison shows that experimental value is very close to theoretical value. For  $\alpha = 0.78$ , THD measured by power analyzer is 16.7%, which shows a good agreement with the theoretical value in Fig. 4.

Fig. 16 shows the transient characteristic of the inverter using proposed controller. At certain delay time after starting,

current magnitude parameter changed from 4A to 9A. As shown, the transient happened near the current peak position which represents the worst case. However, the inverter returns to steady-state quickly with a slight overshoot, while the zero-crossing points are still accurately locked. It shows that the QSW method can be applied to low power or relatively higher power operating conditions and it does not affect the transient performance.

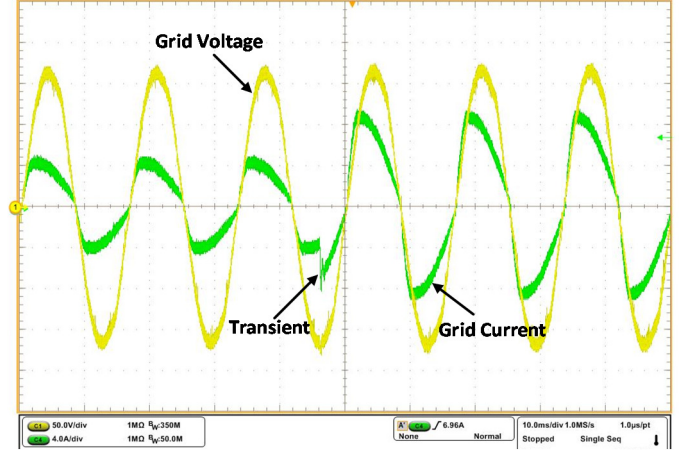


Fig. 16 Transient characteristic when  $\alpha = 0.78$  and current magnitude changes from 4A to 9A.

## VI. CONCLUSIONS

This paper presented a control technique for single phase grid-tie inverters. The control technique allows reactive power injection to unfolding topologies, which were limited to unity power factor operation. The idea was to provide a Quasi Sinusoidal Waveform as a grid current reference to inject reactive power. The mathematical models were provided and explained. A prototype of a unipolar switching full-bridge inverter was built and evaluated for the QSW technique. Working principle of new controller was explained. By comparing measured values and theoretical values, experimental results showed a good agreement with the theory. It was shown that reactive power injection is possible by generating quasi sinusoidal waveform current through the inverter, without changing any hardware components.

## APPENDIX

A. Derivation of (4) – (7): The general equation of a Fourier series is,

$$f(t) = a_0 + \sum_{n=1}^{\infty} \left( a_n \cos \frac{2n\pi t}{T} + b_n \sin \frac{2n\pi t}{T} \right) \quad (A1)$$

By considering the function in (1) and Fig. 2,  $a_0$  is equal to 0 due to no dc offset in the waveform, and

$$a_n = \frac{A}{\pi} \left[ - \int_{-\pi}^{-(1-\alpha)\pi} \sin \frac{\omega t + \pi}{2\alpha} \cdot \cos(n\omega t) \cdot d\omega t \right. \\ + \int_{-\pi}^0 \sin \frac{\omega t}{2(1-\alpha)} \cdot \cos(n\omega t) \cdot d\omega t \\ + \int_{\alpha\pi}^{(1-\alpha)\pi} \sin \frac{\omega t}{2\alpha} \cdot \cos(n\omega t) \cdot d\omega t \\ \left. - \int_{\alpha\pi}^{\pi} \sin \frac{\omega t - \pi}{2(1-\alpha)} \cdot \cos(n\omega t) \cdot d\omega t \right] \quad (A2)$$

$$b_n = \frac{A}{\pi} \left[ - \int_{-\pi}^{-(1-\alpha)\pi} \sin \frac{\omega t + \pi}{2\alpha} \cdot \sin(n\omega t) \cdot d\omega t \right. \\ + \int_{-\pi}^0 \sin \frac{\omega t}{2(1-\alpha)} \cdot \sin(n\omega t) \cdot d\omega t \\ + \int_{\alpha\pi}^{(1-\alpha)\pi} \sin \frac{\omega t}{2\alpha} \cdot \sin(n\omega t) \cdot d\omega t \\ \left. - \int_{\alpha\pi}^{\pi} \sin \frac{\omega t - \pi}{2(1-\alpha)} \cdot \sin(n\omega t) \cdot d\omega t \right] \quad (A3)$$

$a_n$  and  $b_n$  can be determined by simplifying (A2) and (A3), respectively. The resultant equations are as follows,

$$a_n = \frac{2A}{\pi} \cdot \frac{[1-(-1)^n] \cdot (2\alpha-1)}{\{[2n(\alpha-1)]^2-1\} \cdot \{(2n\alpha)^2-1\}} \cdot [1 - 4n^2\alpha(\alpha-1) - 2n \sin(\alpha n\pi)] \quad (A4)$$

$$b_n = \frac{2A}{\pi} \cdot \frac{[1-(-1)^n] \cdot (2\alpha-1)}{\{[2n(\alpha-1)]^2-1\} \cdot \{(2n\alpha)^2-1\}} \cdot 2n \cos(\alpha n\pi) \quad (A5)$$

By using (A1), (A4) and (A5), (4) – (7) can be obtained.

#### B. Derivation of (9) – (10):

By expanding (8),

$$i(t) = \sum_{n=1}^{\infty} I_n (\sin \theta_n \cos n\omega t + \cos \theta_n \sin n\omega t) \quad (A6)$$

By comparing (4) and (A6), two equations can be found as follows,

$$a_n = I_n \sin \theta_n \quad (A7)$$

and 
$$b_n = I_n \cos \theta_n \quad (A8)$$

By solving (A7) and (A8), (9) and (10) can be obtained.

#### REFERENCES

- [1] D. Li, C. Ho, L. Liu, and G. Escobar, "Reactive Power Control for Single-phase Grid-tie Inverters using Quasi Sinusoidal Waveform," *IEEE IECON16*, Nov. 2016.
- [2] S. B. Kjaer, J. K. Pedersen, and F. Blaabjerg, "A review of single-phase grid-connected inverters for photovoltaic modules," *IEEE Trans. on Industry Applications*, vol. 41, no. 5, pp. 1292 – 1306, Sept. 2005.
- [3] Z. Zhao, M. Xu, Q. Chen, J.-S. Lai, and Y. Cho, "Derivation, analysis, and implementation of a boost–buck converter-based high-efficiency PV inverter," *IEEE Trans. on Power Electronics*, vol. 27, no. 3, pp. 1304 – 1313, Mar. 2012.
- [4] U. Prasanna, and A. Rathore "Current-fed interleaved phase-modulated single-phase unfolding inverter: analysis, design, and experimental results," *IEEE Trans. on Industrial Electronics*, vol. 61, no. 1, pp. 310 – 319, Jan. 2014.
- [5] Z. Yang and P. C. Sen, "A novel switch-mode DC-to-AC inverter with nonlinear robust control," *IEEE Trans. on Industrial Electronics*, vol. 45, no. 4, pp. 602-608, Aug 1998.
- [6] M. A. De Rooij, and J. S. Glaser, "High efficiency, multi-source photovoltaic inverter", *US Patent US7929325 (B2)*, 2011-04-19.
- [7] X. Li and A. K. S. Bhat, "A Comparison Study of High-Frequency Isolated DC/AC Converter Employing an Unfolding LCI for Grid-Connected Alternative Energy Applications," *IEEE Trans. on Power Electronics*, vol. 29, no. 8, pp. 3930-3941, Aug. 2014.
- [8] B. Sahan, S. V. Araújo, C. Nöding and P. Zacharias, "Comparative Evaluation of Three-Phase Current Source Inverters for Grid Interfacing of Distributed and Renewable Energy Systems," *IEEE Trans. on Power Electronics*, vol. 26, no. 8, pp. 2304-2318, Aug. 2011.
- [9] P. T. Krein, R. S. Balog, and X. Geng "High-frequency link inverter for fuel cells based on multiple-carrier PWM", *IEEE Trans. on Power Electronics*, vol. 19, no. 5, pp. 1279 – 1288, Sept. 2004.
- [10] A. K. S. Bhat and S. D. Dewan, "Resonant inverters for photovoltaic array to utility interface," *IEEE Trans. on Aerospace and Electronic Systems*, vol. 24, no. 4, pp. 377-386, July 1988.
- [11] C. Rodriguez and G. A. J. Amaratunga, "Long-Lifetime Power Inverter for Photovoltaic AC Modules," *IEEE Trans. on Industrial Electronics*, vol. 55, no. 7, pp. 2593-2601, July 2008.
- [12] Z. Zhao, M. Xu, Q. Chen, J. S. Lai and Y. Cho, "Derivation, Analysis, and Implementation of a Boost–Buck Converter-Based High-Efficiency PV Inverter," *IEEE Trans. on Power Electronics*, vol. 27, no. 3, pp. 1304-1313, March 2012.
- [13] VDE-AR-N 4105, Generators connected to the low-voltage distribution network, 2011.
- [14] X. Su, M. A. S. Masoum and P. J. Wolfs, "Optimal PV Inverter Reactive Power Control and Real Power Curtailment to Improve Performance of Unbalanced Four-Wire LV Distribution Networks," *IEEE Transactions on Sustainable Energy*, vol. 5, no. 3, pp. 967-977, July 2014.
- [15] M. Islam, N. Afrin and S. Mekhilef, "Efficient Single Phase Transformerless Inverter for Grid-Tied PVG System With Reactive Power Control," in *IEEE Transactions on Sustainable Energy*, vol. 7, no. 3, pp. 1205-1215, July 2016.
- [16] T. K. S. Freddy; J. H. Lee; H. C. Moon; K. B. Lee; N. Abd Rahim, "Modulation Technique for Single-Phase Transformerless Photovoltaic Inverters with Reactive Power Capability," in *IEEE Transactions on Industrial Electronics*, 2017.
- [17] "Steca 3600" *Photon – The Solar Power Magazine International*, 9-2011.
- [18] G. Escobar, N. M. Ho, and S. Pettersson, "Method and apparatus for controlling a grid-connected converter", *US Patent US8929108 (B2)*, 2015-01-06.
- [19] T. Weissenhorn, D. Kloos, A. Winter, and Dirk Schekulin "Step-down-converter, DC-AC-converter assembly and method for operating the same", *EU Patent EP2421135A2*, 2012-02-22.
- [20] *Electromagnetic compatibility (EMC) – Part 3-2: Limits – Limits for harmonic current emissions (equipment input current ≤16 A per phase)*, IEC Standard 61000-3-2-2001, 2001.
- [21] G. James, "Chapter 4 - Fourier Series", *Advanced Modern Engineering Mathematics*, 2<sup>nd</sup> Edition, Addison-Wesley, 1999.
- [22] S.-I. Jang and K.-H. Kim, "An islanding detection method for distributed generations using voltage unbalance and total harmonic distortion of current," *IEEE Trans. on Power Delivery*, vol. 19, no. 2, pp. 745-752, April 2004.
- [23] C. A. Canesin and I. Barbi, "Analysis and design of constant-frequency peak-current-controlled high-power-factor boost rectifier with slope compensation," *APEC '96*, 1996, pp. 807-813 vol.2.
- [24] O. Khan and W. Xiao, "An Efficient Modeling Technique to Simulate and Control Submodule-Integrated PV System for Single-Phase Grid Connection," *IEEE Transactions on Sustainable Energy*, vol. 7, no. 1, pp. 96-107, Jan. 2016.
- [25] S. Yang, Q. Lei, F. Z. Peng and Z. Qian, "A Robust Control Scheme for Grid-Connected Voltage-Source Inverters," *IEEE Trans. on Industrial Electronics*, vol. 58, no. 1, pp. 202-212, Jan. 2011.



Dong Li (S'16) received the B.Sc. in electrical engineering and B.Admin. dual degrees from the Tianjin University, Tianjin, China, in 2015. He is currently working toward the Ph.D. degree in electrical engineering in the University of Manitoba, Winnipeg, Canada.

He is currently a Research Assistant at the Laboratory of Renewable-energy Interface and Grid Automation, Department of Electrical and Computer Engineering, University of Manitoba. His research interests include renewable energy interfaces, modularity of power electronic devices and microgrid technologies.



Carl Ngai Man Ho (M'07, SM'12) received the B.Eng. and M.Eng. double degrees and the Ph.D. degree in electronic engineering from the City University of Hong Kong, Kowloon, Hong Kong, in 2002 and 2007, respectively. His Ph.D. research was focused on the development of dynamic voltage regulation and restoration technology.

From 2002 to 2003, he was a Research Assistant at the City University of Hong Kong. From 2003 to 2005, he was an Engineer at e.Energy Technology Ltd., Hong Kong. In 2007, he joined ABB Switzerland. He has been appointed as Scientist, Principal Scientist, Global Intellectual Property Coordinator and R&D Principal Engineer. He has led a research project team at ABB to develop Solar Inverter technologies. In October 2014, he joined the University of Manitoba in Canada as Assistant Professor and Canada Research Chair in Efficient Utilization of Electric Power and established the Renewable Energy Interface and Grid Automation (RIGA) Lab. His research interests are Microgrid technologies, Renewable Energy interfaces, Real

Time Digital Simulation technologies and demand side control methodologies.

Dr. Ho is currently an Associate Editor of the IEEE Transactions on Power Electronics and the IEEE Journal of Emerging and Selected Topics in Power Electronics.



Luo Liu received the Bachelor of Science degree in Electrical Engineering focused on power and energy systems from the University of Manitoba, Winnipeg, Canada, in 2017. He is now studying towards his Master of Science degree in Electrical and Computer Engineering also at the same University.

During the summer term of 2015 and 2016, he was a summer research student in the Department of Electrical and Computer Engineering at the University of Manitoba, where he is working as a research assistant since summer of 2017. His research interests include power electronics and power systems.



Gerardo Escobar (M'02, SM'08) received, in 1999, the Ph.D. degree with honors from the University of Paris Sud XI, CNRS-LSS-SUPELEC in France. From 2009 to 2012 he was a Principal Scientist with the Power Electronics Group, ABB Corporate Research Center, Switzerland. He serves as Associate Editor for IEEE Trans. on Power Electronics since 2013. His main research interests include control of switching power converters, active filters, inverters, electrical drives, and renewable energy systems.